

Transformable Modular Robots: A CPG-Based Approach to Independent and Collective Locomotion

Jiayu Ding, Rohit Jakkula, Tom Xiao, and Zhenyu Gan

Abstract—Modular robotics offers a promising approach for developing versatile and adaptive robotic systems capable of autonomous reconfiguration. This paper presents a novel modular robotic system in which each module is equipped with independent actuation, battery power, and control, enabling both individual mobility and coordinated locomotion. The system employs a hierarchical Central Pattern Generator (CPG) framework, where a low-level CPG governs the motion of individual modules, while a high-level CPG facilitates inter-module synchronization, allowing for seamless transitions between independent and collective behaviors.

To validate the proposed system, we conduct both simulations in MuJoCo and hardware experiments, evaluating the system’s locomotion capabilities under various configurations. We first assess the fundamental motion of a single module, followed by two-module cooperative locomotion. The results demonstrate the effectiveness of the CPG-based control framework in achieving robust, flexible, and scalable locomotion. The proposed modular architecture has potential applications in search-and-rescue operations, environmental monitoring, and autonomous exploration, where adaptability and reconfigurability are essential for mission success.

I. INTRODUCTION

Modular robotics has emerged as a promising approach for developing versatile robotic systems that can dynamically adapt to varying task requirements and environmental constraints [1]–[3]. Unlike conventional single-unit robots with rigid structures and predefined functionalities, modular robots consist of multiple self-contained units that are capable of independent movement and cooperative operation to achieve collective behaviors. These systems demonstrate significant potential in applications requiring adaptability, scalability, and robustness, such as search-and-rescue [4], planetary exploration [5], and autonomous manufacturing and inspection [6], where the ability to reconfigure and recover from failures is critical for mission success.

A key advantage of modular robots is their ability to autonomously reconfigure and self-assemble into different morphologies based on task demands. As illustrated in Fig. 1, a single module is capable of independent operation and wireless communication with other modules, enabling the formation of larger robotic structures with enhanced capabilities. By dynamically assembling into different configurations, modular robots can be adapted for various applications, including search-and-rescue missions, package

Jiayu Ding, Rohit Jakkula, Tom Xiao and Zhenyu Gan are with the Department of Mechanical and Aerospace Engineering, Syracuse University, Syracuse, NY 13244 { jding14, rkjakkul, rxiao14, zgan02}@syr.edu.

This work was supported by a startup fund from the Syracuse University.

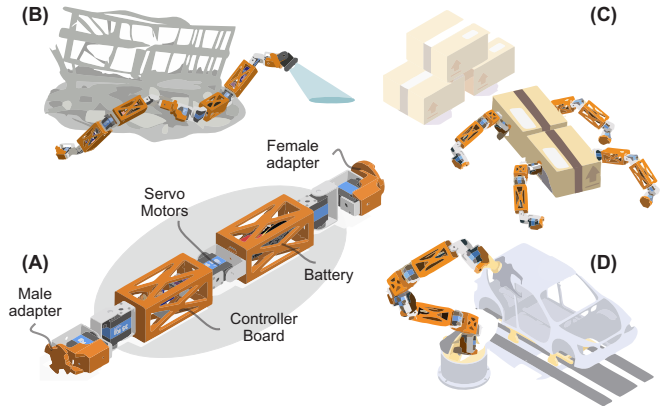


Fig. 1. Overview of the proposed modular robot. (A) A single module operates independently and communicates wirelessly with other modules. By assembling into more complex structures, the system can be adapted for various applications, including (B) search-and-rescue missions, (C) package transportation, and (D) industrial manipulation tasks.

transportation, and industrial manipulation. Existing self-reconfigurable systems such as PolyBot [7], M-TRAN [8], and SMORES-EP [9] have demonstrated significant progress in achieving these capabilities. However, challenges remain in optimizing control strategies that allow seamless transitions between independent and coordinated behaviors.

Incorporating **biologically inspired control mechanisms**, particularly **Central Pattern Generators (CPGs)**, has significantly improved modular robotic locomotion. CPGs, neural networks capable of generating rhythmic patterns, have been widely used in controlling legged and serpentine robots [10]–[14]. Unlike traditional trajectory-based controllers, CPG-based approaches inherently provide robustness against disturbances and adaptability to environmental variations. Recent studies have extended CPG models to modular robots, demonstrating their effectiveness in achieving synchronized locomotion across multiple connected modules [15], [16].

Another critical aspect of modular robotics is **decentralized control and wireless communication**, which enhances system robustness and scalability. Unlike centralized architectures that rely on continuous wired computation and data exchange, decentralized approaches allow individual modules to function autonomously while coordinating with others as needed. This autonomy improves system resilience; if a module malfunctions or becomes damaged, another module can be reprogrammed to assume its role, ensuring continuity in task execution. Such fault tolerance is difficult to achieve in monolithic robot designs, where a single point of failure

can lead to complete system failure [1], [17], [18]. Research in multi-agent communication has explored protocols such as MQTT and UDP to enable real-time synchronization among modules, providing a scalable framework for distributed modular robotic systems.

Building upon these advancements, this paper presents a novel modular robotic system with independent actuation, battery power, and control, allowing each module to function autonomously or as part of a larger coordinated structure. A hierarchical CPG-based control framework is employed, where a low-level CPG governs the motion of individual modules, while a high-level CPG enables inter-module synchronization. This structure allows smooth transitions between independent and collective behaviors, facilitating efficient adaptation to diverse environments. The proposed system is validated through MuJoCo [19] simulations and real-world experiments, showcasing locomotion capabilities across different modular configurations, including single-module movement and two-module cooperative locomotion. Additionally, a preliminary experiment with a four-module configuration is presented in the discussion section.

The remainder of this paper is organized as follows. Section II describes the mechanical design, control architecture, and networking of the modular system. Section III presents experimental validation and simulation results. Finally, Section IV discusses the conclusions and future directions of this research.

II. METHODS

This section describes the design and CPG-based controller implementation of the proposed modular robotic system. Each module is designed to operate independently while also supporting coordinated locomotion through a local Wi-Fi network. This section consists of the mechanical design, actuation system, and embedded control architecture.

A. Modular Robot Design and Networking

The design of the proposed module adheres to the principles of modularity, ease of assembly, and rapid deployment. As shown in Fig. 2(A), the j -th module is modeled as a floating-base system with six degrees of freedom (DoF) at its geometric center, allowing three translational and three rotational motions, represented as $\mathbf{q}_c^j = [x, y, z, q_x, q_y, q_z]^T$. Each module incorporates five actuated joints with angles $\mathbf{q}_b^j = [q_1, q_2, q_3, q_4, q_5]^T$, where each joint operates within the range $[-3/4\pi, 3/4\pi]$ [rad], providing the flexibility needed for both independent locomotion and cooperative transformations. The positive direction is counterclockwise, with zero angles defined when the robot is in its flat configuration, as illustrated in Fig. 2(A). The structural arrangement allows the module to execute a variety of motion primitives, including bending, rotation, and extension, which are essential for both autonomous locomotion and reconfiguration when multiple modules connect and interact. The joint orientations follow a bio-inspired kinematic configuration, balancing flexibility and stability:

- q_1 and q_5 facilitate rolling movements about q_x ,

- q_3 enables lateral pitching motion about q_y ,
- q_2 and q_4 provide primary yaw motion about q_z .

Each joint is actuated by an RDS3235 High Torque Digital Servo [20], a coreless motor servo with all-metal gears, ensuring high durability and precision. The servos operate at a stall torque of 35 kg cm at 7.4 V, providing sufficient actuation strength for both individual locomotion and cooperative transformations. The module's mechanical structure consists of two lightweight frames, 3D-printed using PLA filament, offering a balance between strength, flexibility, and low weight. These frames house the controller board and a 7.4 V, 3000 mAh, 15C 2S Li-ion battery pack, ensuring a compact, modular design while maintaining structural integrity. To enable rapid and secure mechanical coupling, each module is equipped with easy-locking male and female connectors on both ends. These connectors allow for quick attachment and detachment, enabling multiple modules to be assembled into various configurations with minimal effort.

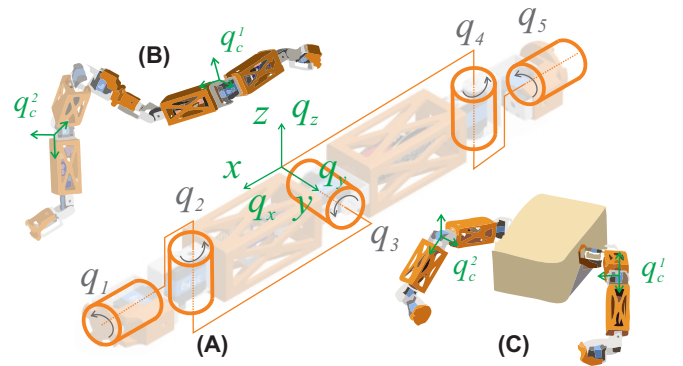


Fig. 2. Kinematic representation of the proposed modular robot. (A) illustrates the floating-base coordinates \mathbf{q}_c and joint angles \mathbf{q}_b of a single module. (B) and (C) depict two possible connection configurations for multi-module assembly.

To achieve real-time coordination, all modules communicate over a Wi-Fi network. Each module is equipped with an ESP32 microcontroller [21], functioning as a slave device responsible for receiving motion trajectories and transmitting feedback. The master controller, implemented on a general-purpose PC, computes desired trajectories at 20 Hz and transmits joint-level commands to each module over Wi-Fi using the MQTT protocol, which enables scalable multi-module coordination. Each ESP32, programmed with MicroPython, processes incoming commands and stores the trajectories asynchronously. A dedicated timer retrieves these trajectories, performs linear interpolation, and generates PWM signals for its servos via a PCA9685 driver [22]. This timer-driven approach allows the servos to execute motions autonomously, eliminating the need for continuous command streaming from the master while maintaining synchronized movement across modules. By leveraging Asyncio, the ESP32 efficiently handles both motion control and system diagnostics in parallel, ensuring reliable multi-tasking.

B. Multilayer CPG Framework

CPGs are neural network-based models that generate rhythmic signals for locomotion control in modular robotic

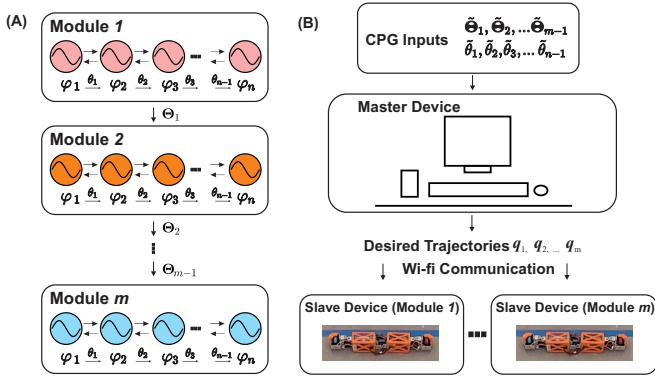


Fig. 3. (A) The two-layer CPG network described in Section II-B. (B) Message passing within the proposed control scheme for modular robots.

systems [15], [16]. In this work, we propose a two-layer CPG framework that integrates both low-level and high-level oscillatory control. The low-level CPG governs the motion of individual modules, ensuring stable periodic actuation, while the high-level CPG coordinates phase relationships across multiple modules to achieve synchronized locomotion. The proposed CPG framework is implemented in Python for both simulation and hardware testing, which is illustrated in Fig. 3.¹

1) *Low-level CPG*: Specifically, each module is driven by an oscillator whose output controls the corresponding motor. Let $\varphi \in \mathbb{R}^n$ be the vector of phase variables associated with n oscillators. These phase variables must be coordinated so that the entire robot exhibits synchronized locomotion. One way to capture the coordination requirement is via the vector of phase differences $\theta \in \mathbb{R}^{n-1}$ defined by

$$\theta = T\varphi, \quad (1)$$

where $T \in \mathbb{R}^{(n-1) \times n}$ is the finite-difference matrix

$$T = \begin{bmatrix} 1 & -1 & 0 & \cdots & 0 \\ 0 & 1 & -1 & \cdots & 0 \\ \vdots & \vdots & \vdots & \ddots & \vdots \\ 0 & 0 & 0 & \cdots & -1 \end{bmatrix}_{(n-1) \times n}, \quad (2)$$

so that $\theta_i = \varphi_i - \varphi_{i+1}$ for $i = 1, \dots, n-1$.

We employ a potential-based *gradient system* approach [23] to achieve a steady-state phase relationship. In this framework, a scalar potential $V(q)$ is defined on a configuration space \mathbb{Q} , and the system evolves via

$$\frac{dq}{dt} = -\frac{\partial V}{\partial q}, \quad (3)$$

driving q toward a minimum $q^* \in \mathbb{Q}$. At q^* , the gradient of V vanishes, and $\frac{\partial^2 V}{\partial q^2} \Big|_{q^*} > 0$, ensuring stable convergence to the desired equilibrium.

¹The full implementation, including source code and documentation, is available in our GitHub repository at: https://github.com/DLARlab/2025_Transformable_Robot.

Following this principle, we introduce an auxiliary coordinate ψ mapped from the phase variables. Define

$$\psi_i = \begin{cases} \varphi_1 - \varphi_2 = \theta_1, & i = 1, \\ \varphi_{n-1} - \varphi_n = \theta_{n-1}, & i = n-1, \\ \varphi_{i+1} + \varphi_{i-1} - 2\varphi_i = \theta_{i-1} - \theta_i, & \text{otherwise.} \end{cases} \quad (4)$$

Given some desired phase-difference configuration $\tilde{\psi}$, we define a quadratic potential function

$$V(\psi) = \sum_{i=1}^{n-1} \mu_i (\psi_i - \tilde{\psi}_i)^2, \quad (5)$$

where $\mu_i > 0$ are convergence coefficients. Imposing the negative gradient of V as the dynamics of ψ guarantees convergence:

$$\frac{d\psi}{dt} = -\nabla_{\psi} V(\psi) = -\left[\frac{\partial V}{\partial \psi_1}, \frac{\partial V}{\partial \psi_2}, \dots, \frac{\partial V}{\partial \psi_{n-1}} \right]^{\top}. \quad (6)$$

Since $\theta = T\varphi$ and ψ is a function of θ (and thus of φ), we can write

$$\frac{d\theta}{dt} = -\left(\frac{\partial \theta}{\partial \psi} \right) \nabla_{\psi} V(\psi) = T \frac{d\varphi}{dt}. \quad (7)$$

Therefore, the dynamic equation of the phases can be derived from $\frac{d\varphi}{dt} = T^{\dagger} \frac{d\theta}{dt}$, where $T^{\dagger} = T^{\top}(TT^{\top})^{-1}$ is the pseudoinverse operator for T . For each oscillator i , the update law can then be written as:

$$\dot{\varphi}_i = \omega_i + A_{i,:} \varphi + B_{i,:} \tilde{\theta}, \quad (8)$$

where ω_i represents the natural (open-loop) oscillation frequency of the i -th oscillator, and $A \in \mathbb{R}^{n \times n}$ and $B \in \mathbb{R}^{n \times (n-1)}$ are coupling matrices. The notation $A_{i,:}$ and $B_{i,:}$ denote the i -th row of their respective matrices. These matrices are defined as:

$$A = \begin{bmatrix} -\mu_1 & \mu_2 & 0 & \cdots & 0 \\ \mu_2 & -2\mu_2 & \mu_2 & \cdots & 0 \\ \vdots & \vdots & \vdots & \ddots & \vdots \\ 0 & 0 & 0 & \cdots & -\mu_n \end{bmatrix}_{n \times n}, \quad B = \begin{bmatrix} 1 & 0 & \cdots & 0 \\ -1 & 1 & \cdots & 0 \\ \vdots & \vdots & \ddots & \vdots \\ 0 & -1 & \cdots & 1 \end{bmatrix}_{n \times (n-1)}. \quad (9)$$

Finally, to generate the actual motor command for the i -th module, we use the oscillator's instantaneous amplitude r_i and phase φ_i according to:

$$\begin{cases} \dot{\varphi}_i = \omega_i + A_{i,:} \varphi + B_{i,:} \tilde{\theta}, \\ \ddot{r}_i = a_i \left[\frac{a_i}{4} (R_i - r_i) - \dot{r}_i \right], \\ q_i = r_i \sin(\varphi_i) + C_i, \end{cases} \quad (10)$$

where R_i is the stable (desired) amplitude, $a_i > 0$ is the convergence rate of the amplitude dynamics, and C_i is a constant offset. This formulation ensures that each oscillator converges to its desired amplitude while maintaining the prescribed phase relationship, thereby producing stable, synchronized rhythmic outputs q_i for the control of the modular robot.

2) *High-Level CPG*: To coordinate the motions among multiple modules, we introduce a high-level CPG layer. Let there be m modules, each containing its own set of oscillators as described in the single-module case. We define a global phase vector $\Phi \in \mathbb{R}^m$, where each entry Φ_j represents the overall (or “high-level”) phase of the j -th module, $j = 1, 2, \dots, m$. Similar to the single-module CPG formulation, we specify a desired phase delay $\tilde{\Theta} \in \mathbb{R}^{m-1}$ at the module level. The actual high-level phase delay Θ is given by

$$\Theta_{j-1} = \Phi_{j-1} - \Phi_j, \quad j = 2, \dots, m, \quad (11)$$

and each Φ_j can be integrated according to a similar dynamic law as in Section II-B.1, ensuring that Φ converges to maintain the desired phase delays Θ .

We can arrange the phases of all oscillators across the m modules into a phase matrix $\mathbf{P} \in \mathbb{R}^{m \times n}$:

$$\mathbf{P} = \begin{bmatrix} \varphi_{1,1} & \varphi_{1,2} & \cdots & \varphi_{1,n} \\ \varphi_{2,1} & \varphi_{2,2} & \cdots & \varphi_{2,n} \\ \vdots & \vdots & \ddots & \vdots \\ \varphi_{m,1} & \varphi_{m,2} & \cdots & \varphi_{m,n} \end{bmatrix}, \quad (12)$$

where each row $[\varphi_{j,1}, \varphi_{j,2}, \dots, \varphi_{j,n}]$ corresponds to the phases of the n oscillators within the j -th module. Note that for a single row j , the difference between consecutive entries is determined by the intra-module phase delay θ . In particular,

$$\varphi_{j,k-1} - \varphi_{j,k} = \theta_k, \quad k = 1, 2, \dots, n. \quad (13)$$

Moreover, to ensure the difference between the $(j-1)$ -th and j -th rows of \mathbf{P} reflects the high-level phase delay Θ_{j-1} , we impose

$$\varphi_{j-1,k} - \varphi_{j,k} = \Theta_{j-1}, \quad k = 1, \dots, n, \quad j = 2, \dots, m. \quad (14)$$

These constraints ensure coherent coordination across both oscillators within a single module (via θ) and modules across the entire system (via Θ).

III. RESULTS

To validate the proposed multi-module CPG framework, we conducted both simulation-based studies and hardware experiments. The MuJoCo physics engine is employed to verify CPG-based control strategies before hardware deployment. Each module is modeled with five actuated joints, driven by the CPG equations derived in Sections II-B.1 and II-B.2. The simulation runs with a timestep of 0.02 seconds, providing sufficient resolution for capturing dynamic interactions, while a friction coefficient of 0.6 is applied to simulate realistic ground contact forces. Desired joint angles are tracked through the PD controller, with the PD gain set up as $K_p = 9000$ and $K_d = 30$, with the damping set to $\epsilon = 150$ [Ns/m] to amplify the servo force output while the maximum possible force was clamped to ensure simulation accuracy to real-world behavior. Throughout the simulations, phase, amplitude, and joint trajectory data are recorded to evaluate system performance in terms of stability, synchronization, and adaptability.

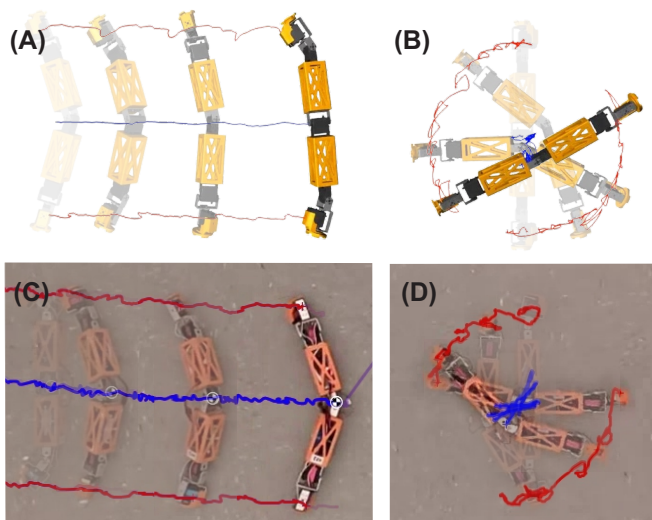


Fig. 4. Keyframes of single-module locomotion in simulation and hardware. (A) and (C): Rolling forward in simulation and physical tests. (B) and (D): Turning in place in both environments.

The study evaluates modular locomotion across multiple configurations, each running for approximately 10 seconds. Single-module tests establish a baseline for independent movement, focusing on lateral rolling and in-place rotation. Two-module coordination is assessed in two setups: a snake-like arrangement for crawling and turning, and a bipedal configuration for forward motion and rotation.

The control system leverages a hierarchical CPG structure to ensure synchronized locomotion across all configurations. High-level phase synchronization between modules, denoted as $\tilde{\theta}_i$, ensures inter-module coordination, while low-level phase coordination within a module, represented by $\tilde{\theta}_{i,j}$, governs intra-module oscillatory behavior. The desired amplitude $R_{i,j}$ and joint offsets $C_{i,j}$ define the range and positioning of limb motions, collectively enabling stable and adaptable locomotion.

A. Single-Module Locomotion: Rolling and Turning in Place

We evaluated the locomotion capabilities of a single module with five actuated joints under two scenarios: rolling forward and turning in place. For both modes, the offset vector was $\mathbf{C} = [0, 0, 0, 0, 0]$ [rad], and the amplitude vector was $\mathbf{R} = [\pi/2, -\pi/2, -\pi/2, \pi/2, \pi/2]$ [rad]. The difference between rolling and turning is defined by the inter-joint phase differences. For rolling forward, all phase differences are set uniformly as $\tilde{\theta}_r = [\pi/2, \pi/2, \pi/2, \pi/2]$ [rad]. For turning in place, alternating phase differences induce counteracting joint motions, given by $\tilde{\theta}_t = [\pi/2, -\pi/2, \pi/2, -\pi/2]$ [rad].

1) *Rolling Forward*: As shown in Fig. 4(A) and (C), when all phase differences are $\pi/2$ [rad] as in $\tilde{\theta}_r$, the module’s limbs move in a wave-like sequence, generating forward propulsion. Across multiple trials, the phase relationships remained stable, with only minor deviations attributed to frictional forces and mechanical tolerances. Both simulation and hardware tests indicate that the rolling speed is proportional

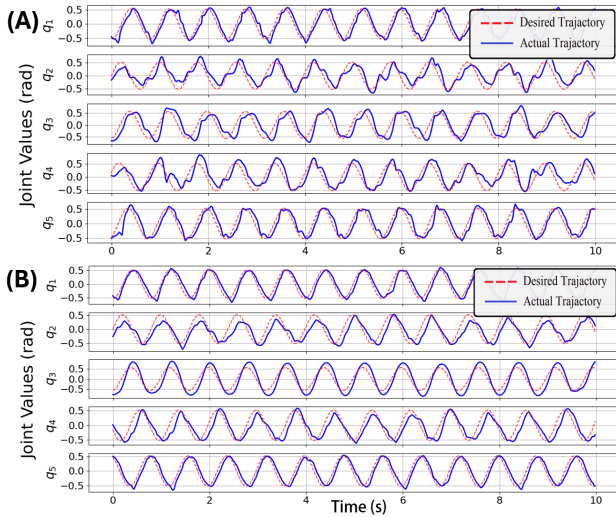


Fig. 5. Comparison of desired (dashed red) and actual (solid blue) joint angles in the MuJoCo simulator for: (A) rolling forward, and, (B) in-place rotation for a single module

to the gait period 1.1 [s]. The maximum observed rolling speed is approximately 0.15 [m/s].

Figure. 5(A) illustrates the joint-level tracking performance observed in the simulation, demonstrating that all five joints closely follow the desired trajectories with minimal deviation. The results indicate stable phase relationships across multiple trials, with tracking errors primarily arising from numerical integration approximations and joint damping effects. The consistency between commanded and actual joint trajectories validates the robustness of the CPG-based control framework in maintaining synchronized oscillatory motion.

2) *Turning in Place*: By alternating the signs in $\tilde{\theta}_t$, the joints produce opposing torques about the module’s center, resulting in controlled rotation around its vertical axis without translational movement. This phase pattern enables the module to achieve in-place turning while maintaining balance and stability. Similar to rolling forward, the joint-level tracking performance in simulation is shown in Figure. 5(B). Throughout multiple trials, the system demonstrated consistent rotational behavior, with minor variations attributed to frictional differences between the contact points and surface irregularities. The turning speed was found to be directly influenced by the gait period, where $T = 1.1$ [s] led to a maximal angular rotation 0.12 [rad/s] while maintaining stable phase synchronization.

B. Two-Module Coordinated Locomotion

To demonstrate multi-module coordination, we connected two modules in two distinct configurations: *snake-like* and *bipedal-like*. In both cases, a high-level phase delay $\tilde{\Theta}$ enforces the relative phase shift between the two modules, while each module’s internal parameters, including amplitude \mathbf{R} , offset \mathbf{C} , and intra-module phase differences $\tilde{\theta}$, are specified accordingly.

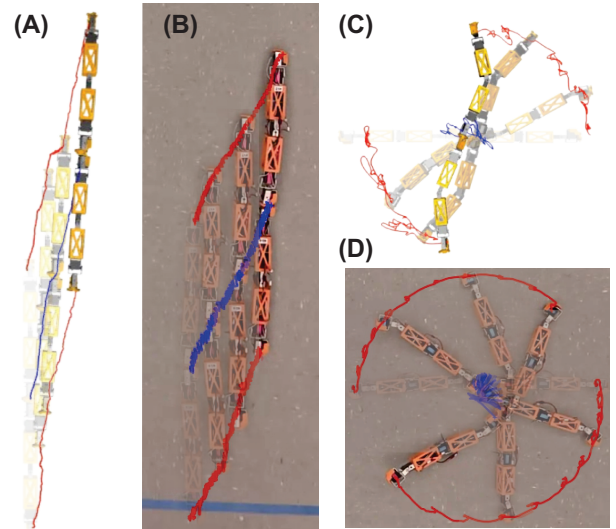


Fig. 6. Keyframes of snake-like two-module locomotion in simulation and hardware. (A) and (B): Crawling motion in simulation and real-world tests. (C) and (D): Turning in place in both environments. Overlaid geometric center and end-effector trajectories confirm effective snake-like motion.

1) *Snake-Like Configuration*: Two modules are connected end-to-end, forming a chain capable of both crawling and turning. The high-level phase delay $\tilde{\Theta}$ synchronizes their movement, ensuring coordinated locomotion.

a) *Crawling Forward Motion*: The intra-module parameters are set as $\tilde{\theta}_s = [\pi/2, \pi/2, -\pi/2, -\pi/2]$ [rad], with amplitudes $\mathbf{R}_s = [0, \pi/4, 0, \pi/4, 0]$ [rad] and offsets $\mathbf{C}_s = [\pi/2, 0, 0, 0, -\pi/2]$ [rad]. Although the motion is not perfectly linear due to asymmetric connections, the chain advances forward efficiently. As shown in Fig. 6(A) and (B), both simulation and hardware tests confirm that the two connected modules effectively propel forward, demonstrating the feasibility of coordinated snake-like locomotion. A forward velocity of 0.03 [m/s] can be achieved on a concrete surface, where the gait period is set to be 2.0 [s] during the testing.

b) *Turning in Place Motion*: The same phase differences are maintained, but the amplitudes to $\mathbf{R}_s = [-\pi/4, \pi/4, -\pi/4, \pi/4, -\pi/4]$ [rad] and offsets are set to $\mathbf{C}_s = [0, 0, 0, 0, 0]$ [rad]. This configuration generates opposing joint movements, causing the entire chain to rotate without significant translation. Figure 6(C) and (D) illustrate the turning motion in both simulation and hardware experiments. The results validate that the proposed CPG framework enables effective in-place rotation for the snake-like configuration, achieving an angular motion at 0.35 [rad/s] at $T = 2.0$ [s].

2) *Bipedal-Like Configuration*: Two modules function as independent limbs, connected to a central torso (a mailing box in our experiments). The high-level phase delay $\tilde{\Theta}$ is set to $\pi/2$ to mimic a walking gait. Due to different mounting orientations, each module is assigned distinct amplitude \mathbf{R} and offset \mathbf{C} values.

a) *Walking Forward Motion*: The intra-module phase differences are set as $\tilde{\theta} = [\pi, 0, -\pi, 0]$ [rad]. The left module has amplitudes $\mathbf{R}_L = [0, \pi/3, \pi/12, 0, 0]$ [rad] and offsets $\mathbf{C}_L = [\pi/2, 0, 0, -\pi/2, -\pi/2]$ [rad], while the

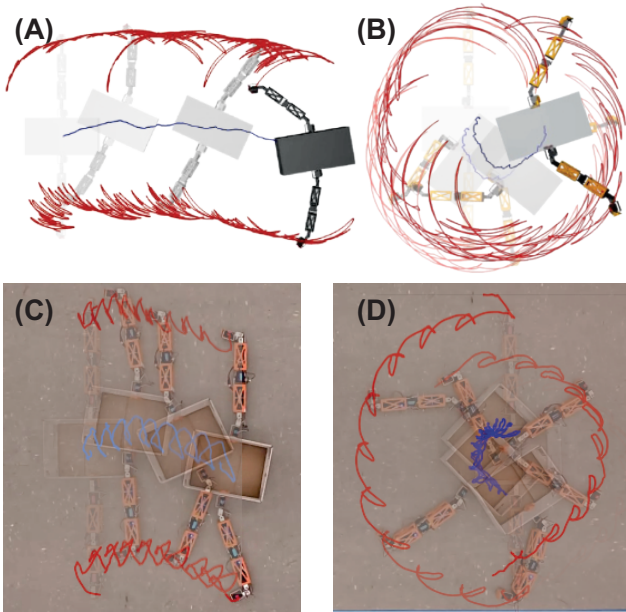


Fig. 7. Keyframes of bipedal-like two-module locomotion in simulation and hardware. (A) and (C): Walking forward motion in MuJoCo and real-world experiments. (B) and (D): Turning in place in both environments. Overlaid center and end-effector trajectories confirm stable limb coordination and adaptability to different module configurations.

right module has $\mathbf{R}_R = [0, \pi/3, -\pi/12, 0, 0]$ [rad] and $\mathbf{C}_R = [-\pi/2, 0, 0, -\pi/2, \pi/2]$ [rad]. These phase settings coordinate the two modules, generating a forward walking motion. Figure 7(A) and (C) illustrate the simulated and real-world results for walking forward. The center and end-effector trajectories confirm that the two-module system maintains a stable, repeatable stride, with a forward velocity of 0.07 [m/s] while remaining the period $T = 1.4$ [s].

b) Turning in Place Motion: The phase differences remain the same, but the right module's amplitude and offset parameters are adjusted to $\mathbf{R}_R = [0, \pi/30, -\pi/120, 0, 0]$ [rad] and $\mathbf{C}_R = [-\pi/2, 0, 0, -\pi/2, \pi/2]$ [rad]. This modification induces asymmetric limb motions, generating a pivot effect that rotates the torso without significant forward displacement. As shown in Fig. 7(B) and (D), the turning motion is successfully achieved in both simulation and hardware. An angular velocity of 0.019 [rad/s] was achieved at a gait period of 1.5 [s].

The results validate that the CPG framework effectively enables both forward and in-place rotation, further demonstrating the adaptability of the bipedal-like configuration.

IV. CONCLUSION AND FUTURE WORK

This paper presents a modular robotic system featuring independent actuation, decentralized control, and a hierarchical CPG-based locomotion framework. Our system enables seamless transitions between autonomous and coordinated behaviors, as validated by extensive simulations and real-world experiments across diverse locomotion scenarios. The results demonstrate that our approach achieves robust, adaptable locomotion while enhancing overall system resilience.

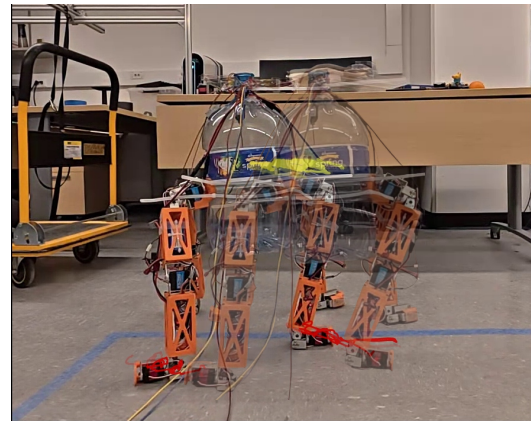


Fig. 8. Four-module coordinated locomotion carrying a water barrel.

In particular, the decentralized communication architecture supports dynamic role reassignment, which improves fault tolerance compared to traditional monolithic designs.

Beyond single- and dual-module configurations, we briefly conducted a four-module coordination experiment. In this experiment, the modules were mounted on a water barrel to perform an object-carrying mission (see Fig. 8). Although the trajectory did not exhibit stable locomotion—largely due to surface distortions of the carried object—the experiment underscores the promising potential of our design for broader applications.

In future work, we plan to extend our framework to larger modular configurations, as demonstrated by the four-module test, and integrate self-reconfiguration capabilities to enhance adaptability in unstructured environments. Furthermore, we intend to leverage reinforcement learning to optimize motion patterns across different modular setups. By deploying a modular network structure [24], we expect to significantly reduce the amount of manual tuning required, thereby further increasing the efficiency and robustness of our locomotion strategies.

REFERENCES

- [1] M. Yim, W.-m. Shen, B. Salemi, D. Rus, M. Moll, H. Lipson, E. Klavins, and G. S. Chirikjian, "Modular self-reconfigurable robot systems [grand challenges of robotics]," *IEEE Robotics & Automation Magazine*, vol. 14, no. 1, pp. 43–52, 2007.
- [2] B. An, S. Miyashita, A. Ong, M. T. Tolley, M. L. Demaine, E. D. Demaine, R. J. Wood, and D. Rus, "An end-to-end approach to self-folding origami structures," *IEEE Transactions on Robotics*, vol. 34, no. 6, pp. 1409–1424, 2018.
- [3] K. Stoy, D. Brandt, and D. Christensen, *Self-Reconfigurable Robots: An Introduction*. MIT Pr; First Edition (January 1, 2010), 01 2010.
- [4] M. Rubenstein, A. Cornejo, and R. Nagpal, "Programmable self-assembly in a thousand-robot swarm," *Science*, vol. 345, no. 6198, pp. 795–799, 2014.
- [5] C. Della Santina, M. G. Catalano, and A. Bicchi, *Soft Robots*. Berlin, Heidelberg: Springer Berlin Heidelberg, 2020, pp. 1–15. [Online]. Available: https://doi.org/10.1007/978-3-642-41610-1_146-2
- [6] A. Pichler, S. C. Akkaladevi, M. Ikeda, M. Hofmann, M. Plasch, C. Wögerer, and G. Fritz, "Towards shared autonomy for robotic tasks in manufacturing," *Procedia Manufacturing*, vol. 11, pp. 72–82, 2017, 27th International Conference on Flexible Automation and Intelligent Manufacturing, FAIM2017, 27-30 June 2017, Modena, Italy. [Online]. Available: <https://www.sciencedirect.com/science/article/pii/S2351978917303438>

- [7] M. Yim, D. Duff, and K. Roufas, "Polybot: a modular reconfigurable robot," in *Proceedings 2000 ICRA. Millennium Conference. IEEE International Conference on Robotics and Automation. Symposia Proceedings (Cat. No.00CH37065)*, vol. 1, 2000, pp. 514–520 vol.1.
- [8] S. Murata, E. Yoshida, A. Kamimura, H. Kurokawa, K. Tomita, and S. Kokaji, "M-tran: Self-reconfigurable modular robotic system," *Mechatronics, IEEE/ASME Transactions on*, vol. 7, pp. 431 – 441, 01 2003.
- [9] J. Davey, N. Kwok, and M. Yim, "Emulating self-reconfigurable robots - design of the smores system," in *2012 IEEE/RSJ International Conference on Intelligent Robots and Systems*, 2012, pp. 4464–4469.
- [10] A. J. Ijspeert, "Central pattern generators for locomotion control in animals and robots: A review," *Neural Networks*, vol. 21, no. 4, pp. 642–653, 2008, robotics and Neuroscience. [Online]. Available: <https://www.sciencedirect.com/science/article/pii/S0893608008000804>
- [11] M. Ajallooeian, S. Pouya, A. Badri-Spröwitz, and A. Ijspeert, "Central pattern generators augmented with virtual model control for quadruped rough terrain locomotion," *Proceedings - IEEE International Conference on Robotics and Automation*, 05 2013.
- [12] T. Mori, Y. Nakamura, M.-A. Sato, and S. Ishii, "Reinforcement learning for a cpg-driven biped robot," in *Proceedings of the 19th National Conference on Artificial Intelligence*, ser. AAAI'04. AAAI Press, 2004, p. 623–630.
- [13] X. Wu and S. Ma, "Cpg-based control of serpentine locomotion of a snake-like robot," *Mechatronics*, vol. 20, no. 2, pp. 326–334, 2010. [Online]. Available: <https://www.sciencedirect.com/science/article/pii/S0957415810000243>
- [14] A. Crespi, D. Lachat, A. Pasquier, and A. Ijspeert, "Controlling swimming and crawling in a fish robot using a central pattern generator," *Autonomous Robots*, vol. 25, 08 2008.
- [15] J. Wang, C. Hu, and Y. Zhu, "Cpg-based hierarchical locomotion control for modular quadrupedal robots using deep reinforcement learning," *IEEE Robotics and Automation Letters*, vol. 6, no. 4, pp. 7193–7200, 2021.
- [16] F. van Diggelen, N. Cambier, E. Ferrante, and A. Eiben, "A model-free method to learn multiple skills in parallel on modular robots," *Nature communications*, vol. 15, no. 1, p. 6267, 2024.
- [17] J. He, Y. Xinhua, Z. Luo, and G. Li, "Backstepping decentralized fault tolerant control for reconfigurable modular robots," *TELKOMNIKA Indonesian Journal of Electrical Engineering*, vol. 11, 07 2013.
- [18] F. Zhou, K. Liu, Y. Li, and G. Liu, "Distributed fault-tolerant control of modular and reconfigurable robots with consideration of actuator saturation," *Neural Computing and Applications*, vol. 32, 09 2020.
- [19] E. Todorov, T. Erez, and Y. Tassa, "Mujoco: A physics engine for model-based control," in *2012 IEEE/RSJ International Conference on Intelligent Robots and Systems*. IEEE, 2012, pp. 5026–5033.
- [20] FEETECH, *RDS3235 High Torque Digital Servo - Specification Sheet*, 2023, accessed: 2025-03-01. [Online]. Available: <https://www.pololu.com/file/0J1434/FT5335M-specs.pdf>
- [21] E. Systems, *ESP32 Series Datasheet: Wi-Fi & Bluetooth SoC*, 2023, accessed: 2025-03-01. [Online]. Available: https://www.espressif.com/sites/default/files/documentation/esp32_datasheet_en.pdf
- [22] N. Semiconductors, *PCA9685: 16-channel, 12-bit PWM Fm+ I2C-bus LED controller*, 2016, accessed: 2025-02-15. [Online]. Available: <https://www.nxp.com/docs/en/data-sheet/PCA9685.pdf>
- [23] Z. Bing, L. Cheng, K. Huang, M. Zhou, A. Knoll, and T. U. M. L. für Rechnertechnik und Rechnerorganisation, *A CPG-based Control Architecture for 3D Locomotion of a Snake-like Robot*, ser. TUM-I. TUM Technische Universität München, Institut für Informatik, 2016.
- [24] W. Huang, I. Mordatch, and D. Pathak, "One policy to control them all: Shared modular policies for agent-agnostic control," 2020. [Online]. Available: <https://arxiv.org/abs/2007.04976>